

# Study of a Tilted Thin Accretion Disk around a Kerr-Taub-NUT black hole

Gargi Sen<sup>1\*</sup>; Chandrachur Chakraborty<sup>2†</sup>; Sudip Bhattacharyya<sup>3‡</sup>;  
 Debaprasad Maity<sup>1§</sup>; Sayan Chakrabarti<sup>1¶</sup>; Santabrata Das<sup>1||</sup>  
<sup>1</sup> *Department of Physics, Indian Institute of Technology Guwahati,  
 Guwahati 781039, India*  
<sup>2</sup> *Manipal Centre for Natural Sciences  
 Manipal Academy of Higher Education, Manipal 576104, India*  
<sup>3</sup> *Department of Astronomy and Astrophysics,  
 Tata Institute of Fundamental Research, Mumbai 400005, India*

## Abstract

The accreting collapsed object GRO J1655-40 could contain the gravitomagnetic monopole (GMM), and it was shown to be better described by the Kerr-Taub-NUT (KTN) spacetime instead of the Kerr spacetime. The warped accretion disk has also been observed for the same collapsed object. Motivated by these, we study a tilted thin inner accretion disk around a slowly-spinning KTN black hole that contains a small GMM. Such a tilting could have a significant effect on the X-ray spectral and timing features via the Lense-Thirring effect. Taking into account the contribution from the inner accretion disk for the KTN black hole, here we calculate the radial profile of a tilt angle. Depending on the numerical values of the viscosity of the accreting material and Kerr parameter, we show that the GMM tends the angular momentum of the disk to align along the black hole's spin axis, or to make it more tilted. Our solution for the radial profile of the tilted disk around a KTN black hole could be useful to probe the strong gravity regime, and could also give indirect evidence for the existence of GMM in nature.

## 1 Introduction

Orbital plane of a test particle around a central rotating object precesses due to the Lense-Thirring (LT) effect [1]. One cannot see such a similar effect in the Schwarzschild spacetime, which apparently indicates that the LT effect arises due to the rotation of the spacetime. If one goes into deeper, one can discover that the 'rotation' is not the fundamental entity responsible for the orbital plane precession. It turns out that the orbital plane precession can arise in any stationary spacetime [2] which violates the time reflection ( $t \rightarrow -t$ ) symmetry but preserves the time translation ( $t \rightarrow t + k$ , where  $k$  is a constant) symmetry [3]. The presence of spin parameter or Kerr parameter ( $a$ ) is responsible to make the Kerr spacetime stationary. In the absence of Kerr parameter, the Kerr spacetime reduces to the Schwarzschild spacetime which is geometrically static and spherically symmetric. If this *non-rotating*

---

\*g.sen@iitg.ac.in

†chandrachur.c@manipal.edu

‡sudip@tifr.res.in

§debu@iitg.ernet.in

¶sayan.chakrabarti@iitg.ernet.in

||sbdas@iitg.ernet.in

Schwarzschild spacetime contains the NUT (Newman-Uni-Tamburino) [4] parameter/charge, it is called as Taub-NUT spacetime which is stationary but spherically symmetric [5]. Thus, one should be able to observe the orbital plane precession in the Taub-NUT spacetime [6], in principle. In this context, one should note here that the orbital plane precession even arises in the magnetized Schwarzschild spacetime [7] (which is static and axisymmetric [8]), surpassing earlier folklore that only a stationary spacetime can generate such a precession. This magnetic field generated phenomenon is known as Gravitational Larmor precession. Thus, it is evident that the orbital plane does not only precess in the stationary and axisymmetric spacetime, but it can also precess if either of them does not hold. However, the NUT charge ( $n$ ) is physically interpreted as ‘a linear source of pure angular momentum’ [9, 10]. The NUT charge is also known as the ‘dual mass’ or gravitomagnetic monopole (GMM) [6].  $n$  is not like the intrinsic angular momentum of a rigid body. It, in fact, gives a ‘rotational sense’ [2] in this spacetime, as it violates the time reflection symmetry. Now, if a Kerr spacetime contains the NUT parameter/GMM, it is called as the Kerr-Taub-NUT (KTN) spacetime. The immediate question arises, how the orbital plane precession or the so-called LT effect is affected due to the presence of an ‘intrinsic rotation’ (i.e.,  $a$ ) and a ‘rotational sense’ (i.e.,  $n$ ). What would be the observational consequences for presence of these two different types of angular momentum parameter.

When a black hole accretes matter from a distant star, an accretion disk is formed around the black hole. The accretion disk formed around a spinning black hole experiences the LT precession. Bardeen and Petterson suggested [11] that the LT effect could change the disk structure around the spinning black hole, if the accretion disk is not in the equatorial plane with respect to the black hole spin axis. Since the LT precession frequency varies with  $R^{-3}$  (where  $R$  is the distance from the central object), the LT torque dominates over the viscous torque of the accreting material close to the black hole. On the other hand, the viscous torque dominates over the LT torque far away from the black hole. The tug-of-war between these two torques divides the accretion disk into three regions. The outer part of the disk remains tilted, the inner part aligns along the equatorial plane due to the strong LT effect and a twisted transition region forms between the above-mentioned two regions. The alignment of the inner accretion disk in the equatorial plane around a spinning black hole is known as the Bardeen-Petterson (BP) effect. The original formulation of Bardeen and Petterson was modified several times by others to remove some inconsistencies [12, 13, 14, 15]. Finally, Pringle [16] successfully introduced a set of equations to describe the BP effect. Later, Scheuer and Feiler [17] introduced the LT effect in the Pringle’s equations and solved the warp disk equation. However, the contribution from the inner accretion disk was not taken into account. Chakraborty and Bhattacharya [18] first analytically solved the full warp disk equation to obtain the expression of tilt angle upto the first order in  $a$  taking into account the inner disk contribution in the warp disk equation derived by Scheuer and Feiler. Banerjee et al. [19] solved the same warp disk equation and showed that the inner disk may not be aligned at all for certain reasonable ranges of parameter values. It was timely because Ingram et al. [20] discovered a tilted inner accretion disk around the black hole H1743-322 from the astrophysical observation. Note that the above-mentioned warped disk scenario has been probed assuming that the black hole is described by the Kerr geometry.

The fundamental cause of the tilted and warped disk is the LT effect or the orbital plane precession which does not appear in the Kerr spacetime only, but it appears in the KTN spacetime also, as discussed earlier. Thus, one can study a tilted thin inner accretion disk around a KTN black hole. This is also important from the astrophysical point of view, as the first clue of the existence of GMM was reported [6] in the astrophysical collapsed object GRO J1655-40 by using the X-ray observational data. It was also shown that GRO J1655-40 could be better described by the KTN spacetime instead of the Kerr spacetime [21]. The warped accretion disk was observed in GRO J1655-40 [22] as well. Primordial black holes [23] and M87\* [24] could also contain GMM. Flattening out of the galaxy rotation curves may be a manifestation of the presence of GMM, without the need of dark matter particles [25, 26].

Thus, one should probe the inner accretion disk around a KTN black hole and find how the inner accretion disk structure is affected due to the presence of both the Kerr parameter and GMM.

Lynden-Bell and Nouri-Zonoz [27] were perhaps the first to argue that the signatures of GMM might be found in the spectra of supernovae, quasars, or active galactic nuclei [6]. However, the existence of GMM has been a subject of debate [28] especially with regard to the closed timelike curve (CTC). Actually, Misner [5] wanted to present an entirely nonsingular cosmological model (homogeneous and anisotropic) with the Taub-NUT metric (described by the mass and GMM) which has a coordinate singularity at  $\theta = \pi$  [29], known as the Misner string. To avoid this string singularity, Misner imposed the time periodicity condition [29, 23] which raises the causality violation issue due to the presence of CTC. Recently, it has been shown [30, 31] that the Taub-NUT spacetime is free from causal pathologies for freely falling observers if the time periodicity condition is not imposed [32, 33], and hence, some longstanding obstructions to accept the Taub-NUT solution as physically relevant are removed [30, 23]. However, as the collapsed object GRO J1655-40 was shown to be better described with the GMM [6, 21], and due to of the availability of the state-of-the-art astrophysical observation facilities now a days, it could be more appropriate to take a practical approach toward understanding the nature of these kind of nonstandard astrophysical backgrounds [28].

Being motivated with all these, in this paper, we study the tilted thin inner accretion disk around a slowly-spinning KTN black hole with a small NUT charge, so that the higher orders of  $a$  and  $n$  can be neglected. In Sec. 2, we discuss the intriguing behavior of the LT effect in the KTN black hole. We describe the basic formalism of the tilted disk in Sec. 3. Our result for the radial profile of the tilted disk is described in Sec. 4. We summarize and conclude in Sec. 5.

## 2 Lense-Thirring precession in Kerr-Taub-NUT spacetime

The KTN metric is expressed here in Schwarzschild-like coordinates  $(t, r, \theta, \phi)$  in the geometrized<sup>1</sup> unit ( $G = c = 1$ ; where  $G$  is the Newtonian gravitational constant and  $c$  is the speed of light in vacuum) [34, 6],

$$ds^2 = -\frac{\Delta}{p^2}(dt - Ad\phi)^2 + \frac{p^2}{\Delta}dR^2 + p^2d\theta^2 + \frac{1}{p^2}\sin^2\theta(adt - Bd\phi)^2, \quad (1)$$

where

$$\begin{aligned} \Delta &= R^2 - 2MR + a^2 - n^2, \\ p^2 &= R^2 + (n + a \cos \theta)^2, \\ A &= a \sin^2 \theta - 2n \cos \theta, \\ B &= R^2 + a^2 + n^2, \end{aligned} \quad (2)$$

with  $M$  is the mass of the spacetime,  $a$  is the Kerr parameter and  $n$  is the NUT parameter. The outer horizon is located at  $R_+ = M + \sqrt{M^2 + n^2 - a^2}$ , and the singularity is located at  $[R = 0, \theta = \cos^{-1}(-n/a)]$  [24].

The exact LT precession frequency ( $\Omega_{\text{LT}}^{\text{KTN}}$ ) for the prograde orbits at  $\theta \rightarrow \pi/2$  in the KTN spacetime is derived as [6]

$$\begin{aligned} \Omega_{\text{LT}}^{\text{KTN}} &= \frac{m^{1/2}}{R^{1/2}(R^2 + n^2) + a m^{1/2}} \left[ 1 - \frac{1}{m^{1/2}(R^2 + n^2)} \times [M(R^6 - n^6 + 15n^4R^2 - 15n^2R^4) \right. \\ &\quad + 2n^2R(3R^4 - 2n^2R^2 + 3n^4) + 16M^2n^2R^3 - 4aR^{1/2}m^{1/2}(n^2 + MR)(n^2 + R^2) \\ &\quad \left. - a^2 \{M(n^4 + 6n^2R^2 - 3R^4) - 8n^2R^3\}^{1/2} \right], \end{aligned} \quad (3)$$

<sup>1</sup>The geometrized unit is considered only in Sec. 2, as it is easy to handle the general relativistic calculation in this unit. The cgs unit is used in the rest of the paper.

where  $m = M (R^2 - n^2) + 2 n^2 R$ . For  $n \rightarrow 0$ , Eq. (3) reduces to [35]

$$\Omega_{\text{LT}} = \frac{M^{1/2}}{(R^{3/2} + aM^{1/2})} \times \left[ 1 - \left( 1 - \frac{4aM^{1/2}}{R^{3/2}} + \frac{3a^2}{R^2} \right)^{1/2} \right], \quad (4)$$

which is well-known expression of the orbital plane precession frequency ( $\Omega_{\text{LT}}$ ) in the Kerr spacetime.

As mentioned earlier, in this work, we study the tilted thin inner accretion disk around a slowly-spinning KTN black hole of mass  $M$  with a small NUT charge/GMM. Thus, let us first write down the expression of  $\Omega_{\text{LT}}^{\text{KTN}}$  (Eq. 3) upto the second order of  $a_*$  ( $\equiv a/M$ ) and  $n_*$  ( $\equiv n/M$ ), *i.e.*,

$$\Omega_{\text{p}} \equiv \Omega_{\text{LT}}^{\text{KTN}} \approx \frac{2a_* M^2}{R^3} - \frac{3a_*^2 M^{5/2}}{2R^{7/2}} - \frac{2n_*^2 M^{3/2}}{R^{5/2}} \times (1 - 2M/R)^2 + \mathcal{O}(a_*^3, n_*^3). \quad (5)$$

The reason to consider upto the second order of both the parameters in Eq. (5) is that the lowest order of NUT parameter appears in the metric (Eq. 1), and thereby in the LT precession frequency expression (Eq. 3) is in the second order. Thus, the minimum requirement is to consider upto the second order of  $n_*$  to see any observable effect of GMM in our study. It is also evident from Eq. (5) that no linear order term of  $n_*$  appears in the expression of  $\Omega_{\text{p}}$ . To compensate  $n_*^2$  in Eq. (5), we consider upto the second order term of Kerr parameter (*i.e.*,  $a_*^2$ ). The first term of Eq. (5) represents the LT precession frequency for the slowly-spinning Kerr black hole. The second term of Eq. (5) represents the precession due to the quadrupole moment of the Kerr black hole [11]. This second term is negligible compared to the first term and might be less important at the large distance (*i.e.*,  $R \gg M$ ) as it varies  $\sim a_*^2/R^{7/2}$ . On the other hand, the third term which corresponds to the LT precession due to the NUT parameter/GMM, dominates over the second term as it varies  $\sim n_*^2/R^{5/2}$ . Intriguingly, the modulus of third term can even dominate over the first term of Eq. (5) depending on the numerical values of  $a_*$ ,  $n_*$  and  $R$ . This indicates that  $\Omega_{\text{p}}$  vanishes at a particular orbit of radius  $R = R_0$ , and the negative LT precession arises for  $R > R_0$ . The negative LT precession in the slowly-spinning KTN black hole arises due to the sole effect of NUT charge [6], and it represents the orbital plane precession in the opposite direction [36]. This intriguing behavior of the LT precession does not arise in case of the Kerr black hole where it follows the inverse cube law of distance ( $\Omega_{\text{LT}} \sim 2a_* M^2/R^3$ ).<sup>2</sup> In case of the KTN black hole, it is evident from Eq. (5) that  $\Omega_{\text{p}}$  does not follow the same law for all combinations of  $(a_*, n_*)$ , and it can even vanish at  $R_0$ . The exact expression of  $R_0$  can be obtained from Eq. (5) by setting  $\Omega_{\text{p}} = 0$  at  $R = R_0$ . As the size of that exact expression is very big, here we write the approximate expression of

$$R_0 \approx \frac{M}{4n_*^4} \left( 2a_*^2 - 3a_*^2 n_*^2 + 16n_*^4 + 2a_* \sqrt{a_*^2 - 3a_*^2 n_*^2 + 16n_*^4} \right), \quad (6)$$

by neglecting  $\sim n_*^2 M^{7/2}/R^{9/2}$  from the last term of Eq. (5) and solve it. The exact numerical value of  $R_0$  differs very small from the approximate value obtained from Eq. (6), if  $R_0$  really occurs close to the order of  $\sim M$ . In most of the cases, the value of  $R_0$  is sufficiently greater than  $M$ . Thus,  $R_0$  gives correct values in those cases<sup>3</sup>.

In accordance with Eq. (5), the LT effect for a slowly-spinning KTN black hole exhibits dominance either by the Kerr parameter ( $a_*$ ) or the NUT parameter/GMM ( $n_*$ ) at any given radial coordinate, as there is a competition between these parameters at  $R$ . To investigate the characteristic behaviors

<sup>2</sup>The negative LT precession arises in the Kerr naked singularity for the range  $R_{\text{ISCO}}^{\text{Kerr}} \leq R < 0.5625a_*^2 M$  [36]. Thus, the value of  $R_0$  in the Kerr spacetime is  $R_0^{\text{Kerr}} = 0.5625a_*^2 M$ . For the Kerr naked singularity, the negative LT precession arises in the orbit(s) of inner disk, whereas it arises in the outer portion ( $R > R_0$ ) of the disk for the KTN black hole.

<sup>3</sup>The exact value of  $R_0$  is not important in this paper. We introduce this only to show how the tilting of the disk depends on this intriguing behavior of LT effect.

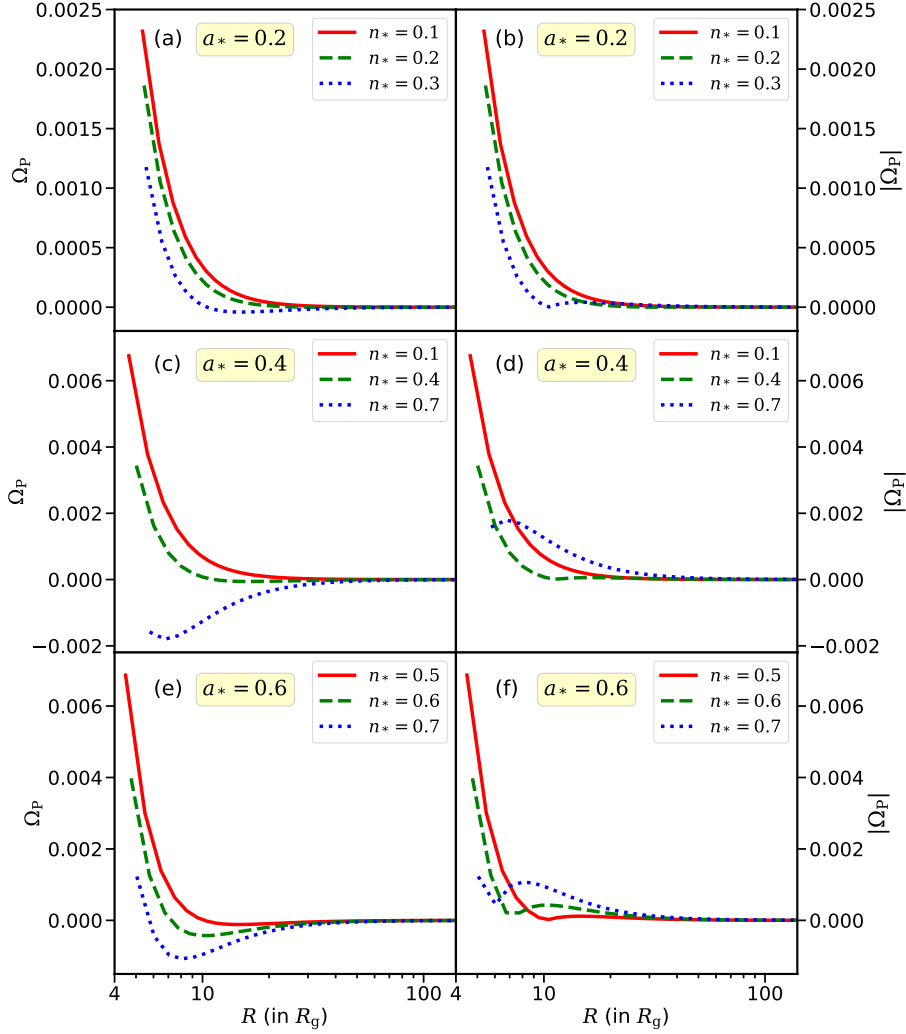


Figure 1: Variation of  $\Omega_p$  (left panel) and  $|\Omega_p|$  (right panel) with radial distance ( $R$ ) for three different values of  $n_*$  with  $a_* = 0.2$  ((a) and (b)),  $a_* = 0.4$  ((c) and (d)), and  $a_* = 0.6$  ((e) and (f)). See § 2 for details.

of  $\Omega_p$  and  $|\Omega_p|$ , we explore three distinct sets of Kerr parameters ( $a_*$ ) in Fig. 1, each followed by three different values of the NUT parameter ( $n_*$ ). This will help us for the comprehensive understanding of the influence of these parameters on the LT frequency and tilted angle of the KTN black hole at a later stage. It is useful to note here that all the curves of Fig. 1 are started from their respective innermost stable circular orbits (ISCOs). The numerical value of the ISCO for a specific combination of ( $a_*$ ,  $n_*$ ) can be obtained by solving the following ISCO equation for prograde orbit [21, 6]

$$M(R^6 - n^6 + 15n^4R^2 - 15n^2R^4) - 2M^2R(3R^4 - 2n^2R^2 + 3n^4) - 16n^4R^3 + 8aR^{3/2}m^{3/2} + a^2 \{M(n^4 + 6n^2R^2 - 3R^4) - 8n^2R^3\} = 0. \quad (7)$$

However, as the LT torque mainly depends on the value of  $\Omega_p$ , we present the corresponding analyses in Fig. 1. In Panels (a) and (b) of Fig. 1, we examine the variations of  $\Omega_p$  and  $|\Omega_p|$ , where the Kerr parameter is set to  $a_* = 0.2$  with NUT parameter values as  $n_* = 0.1$  (red solid line),  $n_* = 0.2$  (green dashed line), and  $n_* = 0.3$  (blue dotted line). Similarly, Panels (c) and (d) of Fig. 1 show the same

variations with  $a_* = 0.4$ , paired with  $n_* = 0.1$  (red solid line),  $n_* = 0.4$  (green dashed line), and  $n_* = 0.7$  (blue dotted line). Panels (e) and (f) of Fig. 1 are illustrated for  $a_* = 0.6$ , along with  $n_* = 0.5$  (red solid line),  $n_* = 0.6$  (green dashed line), and  $n_* = 0.7$  (blue dotted line). These three figures provide a clear depiction of the interplay between GMM and the Kerr parameter on the value of  $\Omega_p$ . The behavior of all the curves of  $|\Omega_p(R)|$  look almost similar. If the value of  $R$  decreases from the outer orbit to the ISCO,  $|\Omega_p(R)|$  first increases, attains a peak, then decreases to zero, and increases again depending on the location of the ISCO. Comparing three sets of figures, we infer that,  $\Omega_p$  or  $|\Omega_p|$  do not follow the same pattern. They depend on the combinations of  $a_*$  and  $n_*$ . Thus, the behavior of the tilted angle of the accretion disk is subject to dependencies on the values of  $a_*$  and  $n_*$  along with the other parameters which we discuss as we proceed.

### 3 Formalism: Tilted and warped disk equation

In our investigation, we focus on a slowly-spinning KTN black hole characterized by a low NUT parameter/GMM at its core. This scenario assumes a Keplerian disk configuration with an aspect ratio  $H/R \ll 1$ , where  $H$  represents the disk thickness and  $R$  signifies the radial distance from the black hole. Notably, the black hole's spin axis aligns with the  $z$  axis and the accretion disk exhibits a tilt concerning the black hole's spin axis. The disk consists of the circular rings with width  $\Delta R$ , surface density  $\Sigma(R, t)$ , and radial velocity  $V_R(R, t)$ . The angular momentum per unit surface area on each annulus of the disk is defined as,  $\mathbf{L}(R, t) = \Sigma R^2 \Omega(R) \mathbf{l}(R, t)$ , where  $\mathbf{l}$  is the unit tilt vector directed normal to the plane of the disk and  $\Omega(R)$  is the Keplerian angular speed. We adopt the assumption of a small tilt angle, implying that  $\mathbf{l}$  can be approximated as  $(l_x, l_y, 1)$ . Additionally, we consider the accretion disk to be sufficiently viscous, satisfying the condition  $\alpha > H/R$ , where  $\alpha$  is the viscosity parameter of standard thin accretion disk [37].

The mass conservation and angular momentum conservation equations [38, 16] can be written as,

$$\frac{\partial \Sigma}{\partial t} + \frac{1}{R} \frac{\partial}{\partial R} (R V_R \Sigma) = 0, \quad (8)$$

and,

$$\frac{\partial}{\partial t} (\Sigma R^2 \Omega) + \frac{1}{R} \frac{\partial}{\partial R} (\Sigma V_R R^3 \Omega) = \frac{1}{R} \frac{\partial}{\partial R} (\nu_1 \Sigma R^3 \Omega') + \frac{1}{R} \frac{\partial}{\partial R} \left( \frac{1}{2} \nu_2 \Sigma R^3 \Omega \frac{\partial \mathbf{l}}{\partial R} \right), \quad (9)$$

where  $\Omega' = d\Omega/dR$ . In the context of accretion disk dynamics,  $\nu_1$  represents the viscosity associated with the azimuthal shear, pertaining to the  $(R, \phi)$  component of shear, while  $\nu_2$  denotes the viscosity linked with the vertical shear, corresponding to the  $(R, z)$  component of shear [38]. The first torque term (also appears for the flat disk, i.e.,  $\partial \mathbf{l} / \partial R = 0$ ) of the right hand side of Eq. (9) acts perpendicular to the disk, whereas the second term operates within the plane only when the disk is warped. The first torque term contributes to the modification of the differential rotation within the plane of the disk, thereby driving the accretion process. Conversely, the second torque term serves to rectify the warp, facilitating the flattening of the disk. The ratio  $\nu_2/\nu_1$ , termed as viscous anisotropy, holds significance in this context and can be associated with  $\alpha$  for small amplitude warps, as evidenced in prior investigations [39]. Here, we assume both these viscosities  $\nu_1$  and  $\nu_2$  are constant. The ratio of  $\nu_2$  and  $\nu_1$  is expressed as [39]

$$\frac{\nu_2}{\nu_1} = \frac{1}{2\alpha^2} \frac{4(1+7\alpha^2)}{4+\alpha^2}. \quad (10)$$

Using Eqs. (8) and (9), the expression for radial velocity ( $V_R$ ) is obtained [16] as,

$$V_R = \frac{\partial / \partial R \left( \nu_1 \Sigma R^3 \Omega' \right) - \frac{1}{2} \nu_2 \Sigma R^3 \Omega |\partial \mathbf{l} / \partial R|^2}{R \Sigma (\partial / \partial R) (R^2 \Omega)}. \quad (11)$$



As we consider the tilt angle is small in this paper, we can neglect the term  $|\partial\mathbf{l}/\partial R|^2$  following [16]. Now, substituting the expression of  $V_R$  (Eq. 11) in Eq. (9), we obtain [16],

$$\frac{\partial\mathbf{L}}{\partial t} = \frac{1}{R} \frac{\partial}{\partial R} \left[ \frac{\frac{\partial}{\partial R} \left\{ \nu_1 \Sigma R^3 (-\Omega') \right\}}{\Sigma \frac{\partial}{\partial R} (R^2 \Omega)} \mathbf{L} \right] + \frac{1}{R} \frac{\partial}{\partial R} \left[ \frac{1}{2} \nu_2 R |\mathbf{L}| \frac{\partial \mathbf{l}}{\partial R} \right] + \frac{1}{R} \frac{\partial}{\partial R} \left[ \nu_1 \left( \frac{R \Omega'}{\Omega} \right) \mathbf{L} \right]. \quad (12)$$

The aforementioned equation delineates the evolution of angular momentum density within an annulus of the thin tilted disk. In case of a Keplerian thin disk around a slowly-spinning black hole, we write

$$\Omega(R) = \sqrt{GM} R^{-3/2}. \quad (13)$$

following [16], and angular momentum as [16],

$$\mathbf{L}(R, t) = \sqrt{GM} R \Sigma \mathbf{l}(R, t). \quad (14)$$

With the help of Eqs. (13) and (14), one obtains

$$\frac{\partial\mathbf{L}}{\partial t} = \frac{1}{R} \frac{\partial}{\partial R} \left[ \frac{3R^{1/2}}{\Sigma} \frac{\partial}{\partial R} \left( \nu_1 \Sigma R^{1/2} \right) \mathbf{L} - \frac{3}{2} \nu_1 \mathbf{L} + \frac{1}{2} \nu_2 R |\mathbf{L}| \frac{\partial \mathbf{l}}{\partial R} \right], \quad (15)$$

from Eq. (12). To account for the relativistic effects induced by the presence of a KTN black hole, we extend Eq. (15) to incorporate the external torque arising from the LT precession. Following [17, 16], we remove the time dependent term of the left hand side of Eq. (15), and add the external torque to the right-hand side as the effective couple due to the LT precession. The external torque ( $\boldsymbol{\tau}$ ) due to the LT precession is given by,

$$\boldsymbol{\tau} = \boldsymbol{\Omega}_p \times \mathbf{L}, \quad (16)$$

where  $\boldsymbol{\Omega}_p$  in the cgs unit is written as (see Eq. 5),

$$\boldsymbol{\Omega}_p = \frac{c}{R} \left( \frac{2a_* R_g^2}{R^2} - \frac{3a_*^2 R_g^{5/2}}{2R^{5/2}} - \frac{2n_*^2 R_g^{3/2}}{R^{3/2}} (1 - 2R_g/R)^2 \right), \quad (17)$$

where  $R_g (= GM/c^2)$  is the gravitational radius.

In this paper, our focus lies in investigating the effect of both the viscous and LT torques within the disk in a steady state. Thus, the evolution equation (Eq. 15) in the steady state ( $\partial\mathbf{L}/\partial t = 0$ ) can be expressed as follows [17],

$$\frac{1}{R} \frac{\partial}{\partial R} \left[ \left( \frac{3R}{L} \frac{\partial}{\partial R} (\nu_1 L) - \frac{3}{2} \nu_1 \right) \mathbf{L} + \frac{1}{2} \nu_2 R L \frac{\partial \mathbf{l}}{\partial R} \right] + (\boldsymbol{\Omega}_p \times \mathbf{L}) = 0. \quad (18)$$

Taking the scalar product of  $\mathbf{l}$  [17] with Eq. (18), we get

$$\frac{1}{R} \frac{\partial}{\partial R} \left[ R \frac{\partial}{\partial R} (\nu_1 L) - \frac{1}{2} \nu_1 L \right] = 0, \quad (19)$$

under the small tilt angle approximation (we have ignored the term  $|\partial\mathbf{l}/\partial R|^2$ ). Solving the above equation, one obtains [17],

$$L(R) = C_2 R^{1/2} - 2C_1, \quad (20)$$

where  $C_1$  and  $C_2$  are the integration constants. They are obtained as  $C_2 = \sqrt{GM} \Sigma_\infty$  and  $C_1 = \frac{1}{2} \sqrt{GM R_{\text{in}}} (\Sigma_\infty - \Sigma_{\text{in}})$  [18], where  $\Sigma \rightarrow \Sigma_\infty$  at  $R \rightarrow \infty$  and  $\Sigma \rightarrow \Sigma_{\text{in}}$  at  $R \rightarrow R_{\text{ISCO}}$ . Here,  $R_{\text{in}}$

corresponds to the inner edge radius of the disk, that is, in fact, the ISCO radius ( $R_{\text{in}} \equiv R_{\text{ISCO}}$ ) for a KTN black hole. Note that one can obtain  $R_{\text{ISCO}}$  by solving Eq. (7). Finally, substituting the above expressions for  $C_1$  and  $C_2$  into Eq. (20), we obtain the expression for  $L(R)$  in steady state as,

$$L(R) = \sqrt{GM} \left[ R^{1/2} \Sigma_{\infty} + R_{\text{in}}^{1/2} (\Sigma_{\text{in}} - \Sigma_{\infty}) \right]. \quad (21)$$

The steady state distribution of the surface density can similarly be obtained from Eq. (21) upon substituting the right hand side expression of Eq. (14) as

$$\Sigma(R) = \Sigma_{\infty} + (R_{\text{in}}/R)^{1/2} (\Sigma_{\text{in}} - \Sigma_{\infty}). \quad (22)$$

Now, substituting  $L(R)$  in Eq. (18) we obtain,

$$\frac{1}{R} \frac{\partial}{\partial R} \left[ 3\nu_1 C_1 \mathbf{l} + \frac{1}{2} \nu_2 R L \frac{\partial \mathbf{l}}{\partial R} \right] + (\boldsymbol{\Omega}_p \times \mathbf{l}) = 0. \quad (23)$$

Eq. (23) can be decomposed into  $x$  and  $y$  components (i.e.,  $l_x$  and  $l_y$ ) of the tilt vector ( $\mathbf{l}$ ) as

$$\frac{\partial}{\partial R} \left( 3\nu_1 C_1 l_x + \frac{1}{2} \nu_2 R L \frac{\partial l_x}{\partial R} \right) = \omega_p L l_y, \quad (24)$$

and

$$\frac{\partial}{\partial R} \left( 3\nu_1 C_1 l_y + \frac{1}{2} \nu_2 R L \frac{\partial l_y}{\partial R} \right) = -\omega_p L l_x, \quad (25)$$

where  $\boldsymbol{\omega}_p \times \mathbf{l} = (-\omega_p l_y, \omega_p l_x, 0)$  and  $\omega_p = c \left( \frac{2a_* R_g^2}{R^2} - \frac{3a_*^2 R_g^{5/2}}{2R^{5/2}} - \frac{2n_*^2 R_g^{3/2}}{R^{3/2}} (1 - 2R_g/R)^2 \right)$ .

Combining Eqs. (24) and (25), we obtain

$$\frac{\partial}{\partial R} \left( 3\nu_1 C_1 W + \frac{1}{2} \nu_2 R L \frac{\partial W}{\partial R} \right) = -i\omega_p L W, \quad (26)$$

where we define  $W = l_x + il_y = \beta e^{i\gamma}$  with  $\beta = \sqrt{l_x^2 + l_y^2}$  is the tilt angle and  $\gamma = \tan^{-1}(l_y/l_x)$  is the twist angle. Eqs. (24) and (25) refer the evolution and characteristics of the warped disk around a KTN black hole in the steady state.

Here, we use the dimensionless form of some parameters for our convenience in the mathematical calculations. For instance, the dimensionless form for  $L$  [19] is given by  $L \rightarrow L/C_1 = (C\sqrt{R} - 2)$ , where  $C = \frac{2z_{\text{in}}}{z_{\text{in}} - 1} \frac{1}{\sqrt{R_{\text{in}}}}$  and  $z_{\text{in}} = 1 + \frac{2C_1}{L(R_{\text{in}})} = \frac{\Sigma_{\infty}}{\Sigma_{\text{in}}}$  [19]. We make  $R$  dimensionless by replacing  $R \rightarrow \frac{R}{R_g}$ ,  $\xi \rightarrow \frac{cR_g}{\nu_2}$  and  $\eta \rightarrow \frac{6\nu_1}{\nu_2}$ . Using the above-mentioned scheme and by following [19], we obtain the dimensionless form of Eqs. (24) and (25) as

$$R \frac{\partial^2 l_x}{\partial R^2} + \left[ (\eta + 1) \frac{C_1}{L} + 3/2 \right] \frac{\partial l_x}{\partial R} = \frac{2\omega_{\text{LT}}^{\text{KTN}} l_y}{\nu_2} = 2\xi \bar{\omega} l_y, \quad (27)$$

and

$$R \frac{\partial^2 l_y}{\partial R^2} + \left[ (\eta + 1) \frac{C_1}{L} + 3/2 \right] \frac{\partial l_y}{\partial R} = -\frac{2\omega_{\text{LT}}^{\text{KTN}} l_x}{\nu_2} = -2\xi \bar{\omega} l_x. \quad (28)$$

where,

$$\bar{\omega} = \left( \frac{2a_*}{R^2} - \frac{3a_*^2}{2R^{5/2}} - \frac{2n_*^2}{R^{3/2}} (1 - 2/R)^2 \right). \quad (29)$$



Now, we solve Eqs. (27) and (28) numerically with proper boundary conditions to see the behaviour of  $\beta$  for various parameters. To solve the above-mentioned warped disk equations (Eqs. 27 and 28), we need four boundary conditions, which are taken as

$$l_x(R_{\text{in}}) = \beta_i \cos(\gamma_i), \quad l_y(R_{\text{in}}) = \beta_i \sin(\gamma_i), \quad (30)$$

and,

$$l_x(R_f) = \beta_f, \quad l_y(R_f) = 0 \quad (31)$$

following [19]. We define several key parameters:  $R_f$ ,  $\gamma_i$ ,  $\beta_i$ , and  $\beta_f$ , representing the outer edge radius, twist angle at the inner boundary, tilt angle at the inner edge, and tilt angle at the outer edge of the disk, respectively. At the outer edge of the disk, we assume the twist angle to be zero since the effect of LT precession is negligible there. Consequently,  $l_y$  can be assumed to be zero at the outer edge. The inner edge of the disk is  $R_{\text{in}}$ , which is the ISCO radius ( $R_{\text{ISCO}}$ ) for a prograde disk, as mentioned earlier.

## 4 Result

In this section, we investigate the behavior of the tilt angle radial profile ( $\beta(R)$ ) as a function of the parameters  $a_*$ ,  $n_*$ ,  $\beta_i$ ,  $\nu_2$ , and  $\eta$  in detail. In case of the Kerr black hole, it was earlier shown [19] that the interplay between the LT torque (controlled by  $M, a_*, \beta_i$ ) and viscous torque (controlled by  $\nu_2$ ) in the plane of the disk decides the radial profile of  $\beta$ . In case of the KTN black hole, the LT torque is additionally controlled by  $n_*$  as well. In Sec. 2, we have shown that the LT effect (Eq. 5) can decrease or increase or even vanish at a particular orbit ( $R_0$ ) depending on the values of  $a_*$  and  $n_*$ . The similar effect does not arise for the Kerr black hole. In case of the KTN black hole, although there is certainly an interplay between the LT torque and viscous torque, one cannot neglect another interplay between  $a_*$  and  $n_*$  inside the LT torque. Due to the interplay between three primary parameters ( $a_*$ ,  $n_*$  and  $\nu_2$ ), some peculiar effect will appear around  $R_0$  (not exactly at  $R_0$ ), which we discuss as we proceed.

In order to discuss the behavior of  $\beta(R)$ , we need to choose the suitable numerical values for the different parameters relevant for the astrophysical scenario. As we are mainly interested in the Galactic accreting black holes, we choose  $M \sim 5 - 15M_\odot$  (where  $M_\odot$  is the solar mass) [40] for most of the cases. The value of  $\nu_2$  is considered as  $10^{14} - 10^{15} \text{ cm}^2 \text{ s}^{-1}$  [41].  $\eta$  is chosen as  $\eta \sim 0.0012 - 0.94$ , which translates to the range  $0.01 - 0.4$  for  $\alpha$  [42]. We consider a range of  $0.3 - 0.75$  for  $z_{\text{in}}$ , as in our formalism  $\Sigma_{\text{in}} > \Sigma_\infty$ . The inner edge twist and outer edge tilt to  $\sim 5^\circ$  and  $\sim 10^\circ$  respectively throughout the paper. We consider  $\beta_i$  as a free parameter following [23, 19], and use the range  $0^\circ - 10^\circ$  for the purpose of demonstration. Note that we consider only the case of prograde rotation ( $a_* > 0$ ) in this paper.

Fig. 2 is plotted for  $a_* = 0.4$  with the three different values of  $n_*$ :  $n_* = 0.3$  (red solid line),  $n_* = 0.4$  (green dashed line), and  $n_* = 0.5$  (blue dotted line). The values of  $R_0$  are  $\sim 24.5R_g, 11.3R_g$  and  $7.3R_g$  for the combinations of  $(a_*, n_*) \equiv (0.4, 0.3), (0.4, 0.4)$  and  $(0.4, 0.5)$ , respectively. When transitioning from left to right  $[(a \rightarrow b), (c \rightarrow d)]$ , we maintain a constant value for  $\nu_2$  while varying  $M$  from  $5M_\odot$  to  $10M_\odot$ . Conversely, moving from the upper to the lower arrangement  $[(a \rightarrow c), (b \rightarrow d)]$ , we keep the mass  $M$  fixed and adjust the viscosity parameter  $\nu_2$  from  $5 \times 10^{14} \text{ cm}^2 \text{ s}^{-1}$  to  $10^{15} \text{ cm}^2 \text{ s}^{-1}$ , with all other parameters held constant. In this analysis, it becomes apparent that for a fixed combination of  $a_*$ ,  $n_*$ , and  $\nu_2$ , the LT torque amplifies with an increase in  $M$ , so it will help to align the angular momentum of the disk with the spin direction. Conversely, with a consistent set of  $a_*$ ,  $n_*$ , and  $M$ , the viscous torque increases as  $\nu_2$  increases. Consequently, higher values of  $\nu_2$  lead to greater misalignment of the disk relative to the spin axis.

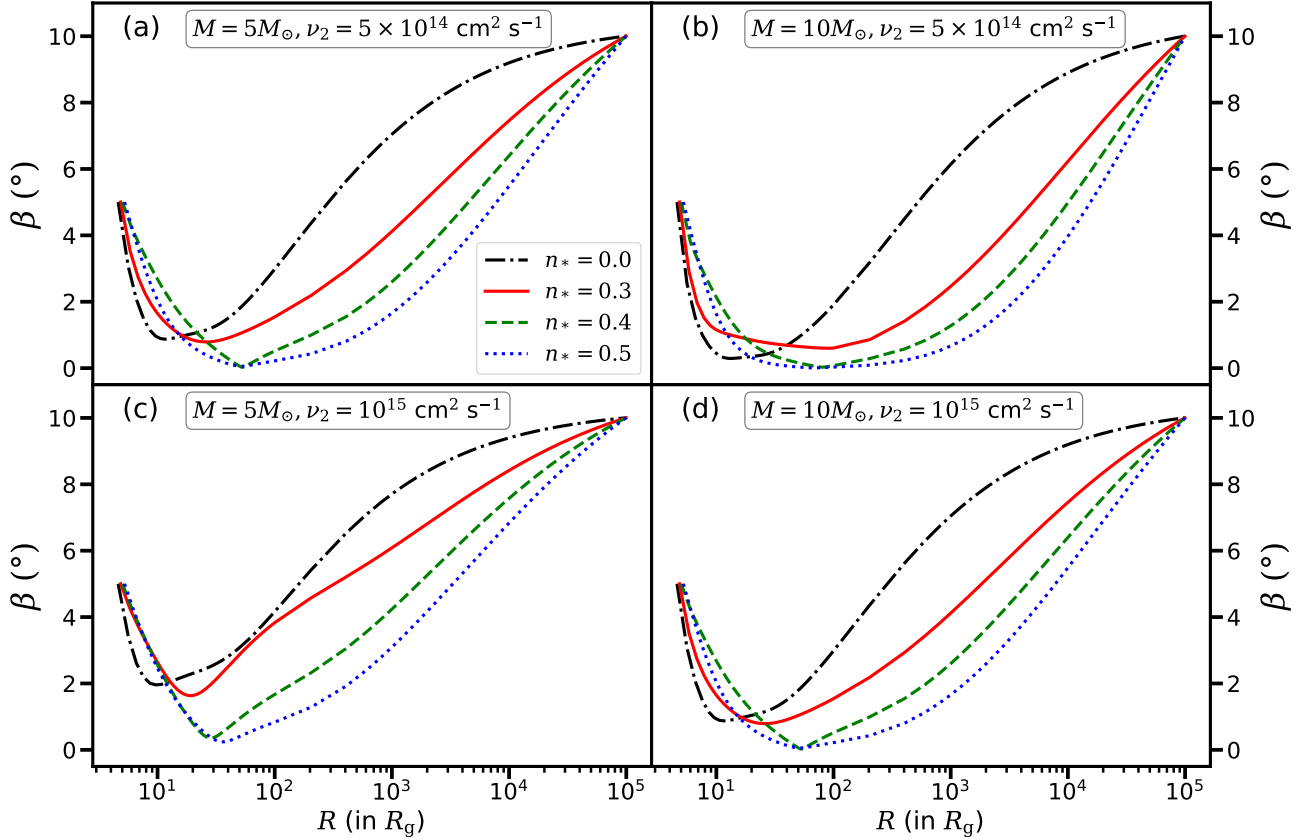


Figure 2: Variation of tilt angle ( $\beta$ ) with radial distance ( $R$ ) for three different values of  $n_*$  with a fixed value of  $a_* = 0.4$ ,  $\beta_i = 5^\circ$ ,  $\eta = 0.25$  and  $z_{\text{in}} = 0.75$ . The value of  $M$  ( $\nu_2$ ) is fixed in the plots of 1st/2nd column (row) with different values of  $\nu_2$  ( $M$ ) as mentioned in the inset. All the curves are started from  $R_{\text{in}} \equiv R_{\text{ISCO}}(a_*, n_*)$  which are calculated using Eq. (7). See § 4 for details.

Fig. 3 illustrates the variation of  $\beta$  with respect to the radial coordinate for different values of  $\nu_2$ . The upper-left figure corresponds to  $\nu_2 = 10^{14} \text{ cm}^2 \text{ s}^{-1}$ , the upper-right figure to  $\nu_2 = 5 \times 10^{14} \text{ cm}^2 \text{ s}^{-1}$ , the lower-left figure to  $\nu_2 = 10^{15} \text{ cm}^2 \text{ s}^{-1}$ , and the lower-right figure to  $\nu_2 = 5 \times 10^{15} \text{ cm}^2 \text{ s}^{-1}$ . The various curves within each figure represent different values of the Kerr parameter ( $a_*$ ), ranging from 0.0 to 0.8 with an interval of  $\Delta a_* = 0.1$ . It is notable that higher values of  $a_*$  tend to align the angular momentum of the disk along the black hole's spin axis, resulting in smaller values of  $\beta$ . Observing the plots, it becomes evident that as the value of  $\nu_2$  increases, the viscous torque begins to dominate over the Lense-Thirring torque for a fixed set of  $(a_*, n_*)$ . The competition between viscous and Lense-Thirring torques plays a crucial role in determining the orientation of the accretion disk, with higher values of  $\nu_2$  exerting a greater influence on the disk's inclination relative to the black hole's spin axis.

Fig. 4 depicts the variation of the tilt angle ( $\beta$ ) with radial distance ( $R$ ) for different values of  $\nu_2$  but similar to Fig. 3. The various curves in each panel represent different values of  $n_*$ , ranging from 0.0 to higher values with an interval of  $\Delta n_* = 0.1$  with a fixed value of  $M = 10 M_\odot$  and  $a_* = 0.3$ . For  $\nu_2 = 10^{14} \text{ cm}^2 \text{ s}^{-1}$ , the disk remains mostly aligned along the equatorial plane for any values of  $n_*$ . For  $\nu_2 = 5 \times 10^{14} \text{ cm}^2 \text{ s}^{-1}$ , the disk tends to align along the equatorial plane for  $n_* > 0.4$ . For  $\nu_2 = 10^{15} \text{ cm}^2 \text{ s}^{-1}$ , the disk aligns beyond  $n_* > 0.5$ , while for  $\nu_2 = 5 \times 10^{15} \text{ cm}^2 \text{ s}^{-1}$ , the disk remains mostly tilted

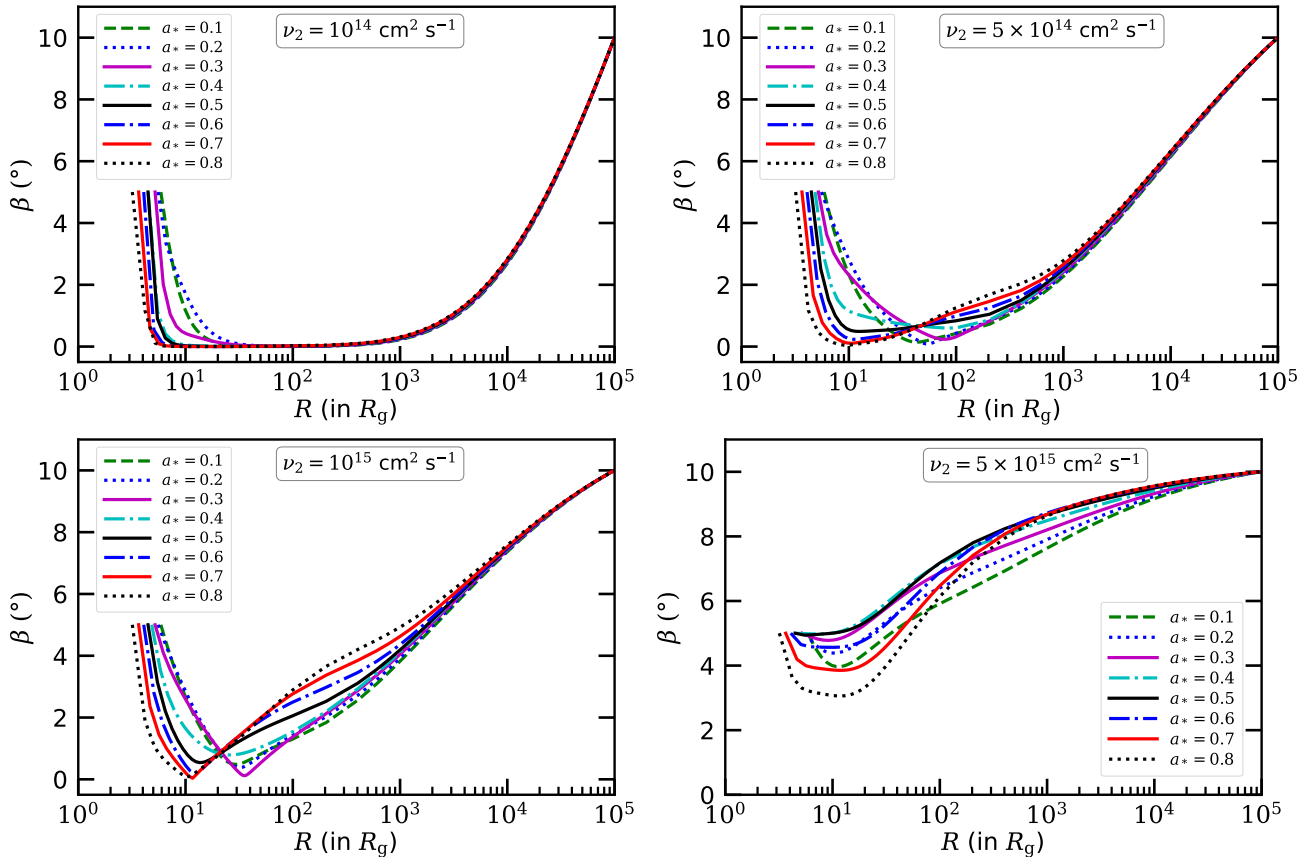


Figure 3: Variation of  $\beta$  with  $R$  for the different values of  $a_*$  with a fixed value of  $M = 10M_\odot$ ,  $\beta_i = 5^\circ$ ,  $n_* = 0.3$ ,  $\eta = 0.25$  and  $z_{\text{in}} = 0.75$ . The value of  $\nu_2$  changes in the plots as mentioned in the inset. All the curves are started from  $R_{\text{in}} \equiv R_{\text{ISCO}}(a_*, n_*)$  which are calculated using Eq. (7). See § 4 for details.

for any values of  $n_*$ . Here also, as the value  $\nu_2$  increases, the viscous torque starts to dominate over the LT torque for a fixed set of  $(a_*, n_*)$ . In all the panels of Fig. 4, the solid magenta curve shows the tilt profile for  $a_* = n_*$ . Remarkably, the curves for  $n_* < a_*$  are located at the upper portion of the  $xy$  plane, whereas the curves are located at the lower portion of the same plane for  $n_* > a_*$ . This indicates that the LT torque becomes stronger for the higher value of  $n_*$ . This does not only help to align the disk in the equatorial plane, but the alignment of the disk is also extended to the outer portion of the disk significantly. This could be clear by comparing the first and last terms of Eq. (5), as it varies  $\sim a_*/R^3$  and  $\sim n_*^2/R^{5/2}$  respectively. In the absence of  $n_*$  (red dotted curve), the disk might be aligned in the equatorial plane for small viscosity (see panel (a)), but it is not aligned for the comparatively higher viscosity (see panels (b)-(d)). It is evident from panels (a)-(d) that there is a tendency of the alignment of disk in the equatorial plane for the higher values of  $n_*$ . It indicates that the higher values of  $n_*$  play a significant role for the alignment, comparing to  $a_*$ . It is because the last term ( $\sim n_*^2/R^{5/2}$ ) of Eq. (5) dominates over the first and second terms of the same equation. It is interesting to see the behavior of the dotted blue curves in panels (b) and (c) of figure 4. As the difference between the value of  $a_*$  (e.g.,  $a_* = 0.3$ ) and  $n_*$  (e.g.,  $n_* = 0.2$ ) is small ( $\sim 0.1$ ), the overall LT torque remains small for  $R < 100R_g$  and  $R < 300R_g$  for panels (b) and (c), respectively. Note that  $R_0$  occurs at  $R_0 \sim 60R_g$  for  $(a_*, n_*) = (0.3, 0.2)$ . Thus, the viscous torque dominates over the LT torque and the disk tends to be more tilted compared to the dashed green and dotted red curves around  $R_0$ . On the other hand, the

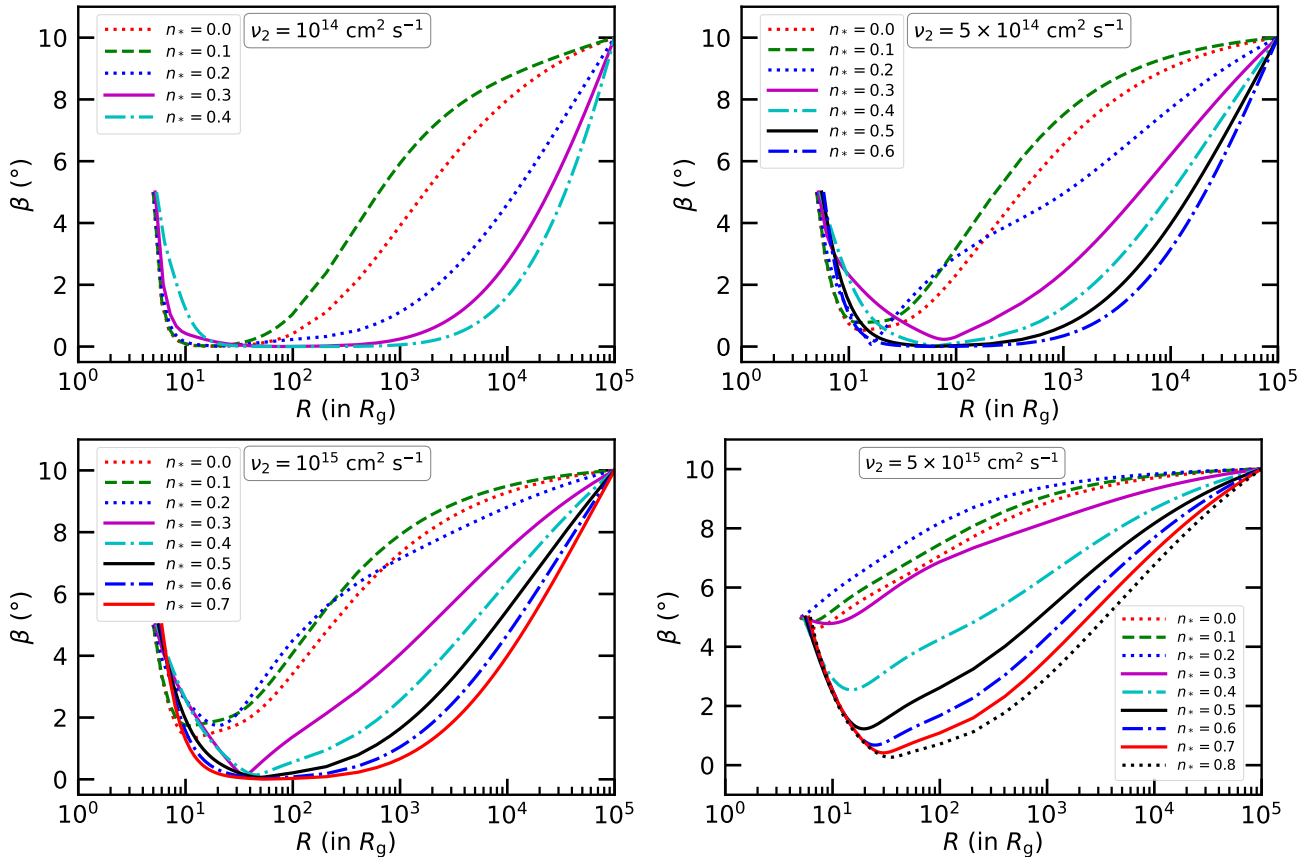


Figure 4: Variation of  $\beta$  with  $R$  for different values of  $n_*$  with a fixed  $a_* = 0.3$ ,  $M = 10M_\odot$ ,  $\eta = 0.25$ ,  $\beta_i = 5^\circ$  and  $z_{\text{in}} = 0.75$ . The value of  $\nu_2$  changes in the different panels as mentioned in the inset. See § 4 for details.

LT torque due to  $n_*$  starts to dominate over the LT torque due to  $a_*$  for the larger  $R$ , and, hence, the overall torque dominates over the viscous torque. Thus, the disk tries to be aligned and, thereby the dotted blue curves bent and crosses the dashed green and dotted red curves at larger  $R$  in panels (b) and (c). The dotted blue curve in panel (d) indicates that the viscous torque dominates over the overall LT torque almost the whole range of  $R$ . Thus, one cannot see the tendency of disk alignment.

Fig. 5 portrays the variation of  $\beta$  with respect to the radial coordinate for different values of  $\nu_2$  with some fixed parameters:  $M = 10M_\odot$ ,  $\eta = 0.25$  and  $z_{\text{in}} = 0.75$ . The upper-left and upper-right figures depict scenarios where  $(a_*, n_*) = (0.3, 0.5)$  with  $\beta_i = 5^\circ$  and  $0^\circ$ , respectively. Similarly, the lower-left and lower-right figures represent cases with  $(a_*, n_*) = (0.5, 0.3)$  with  $\beta_i$  values of  $5^\circ$  and  $0^\circ$ , respectively. Studying all the panels, we can infer that, the inner disk is more tilted for large  $\beta_i$ . Moreover, it is also seen that the tilting of the disk increases with the increment of  $\nu_2$ .

Fig. 6 showcases the variation of  $\beta$  with respect to the radial coordinate for different values of  $M$ . Here we fix  $\nu_2 = 5 \times 10^{14} \text{ cm}^2 \text{ s}^{-1}$ ,  $\eta = 0.25$  and  $z_{\text{in}} = 0.75$ . The upper-left and upper-right figures correspond to scenarios where  $(a_*, n_*) = (0.3, 0.5)$  with  $\beta_i = 5^\circ$  and  $0^\circ$ , respectively. Similarly, the lower-left and lower-right figures represent cases with  $(a_*, n_*) = (0.5, 0.3)$ , with  $\beta_i = 5^\circ$  and  $0^\circ$ , respectively. Across all the subfigures, it is observed that the LT torque dominates for higher black hole masses. This observation highlights the significance of the black hole mass in determining the dominance of the LT torque and its effect on aligning the accretion disk with the black hole's spin axis.

Fig. 7 is similar to Fig. 6 but for a different value of  $\nu_2$ , i.e.,  $\nu_2 = 10^{15} \text{ cm}^2 \text{ s}^{-1}$ . Comparing

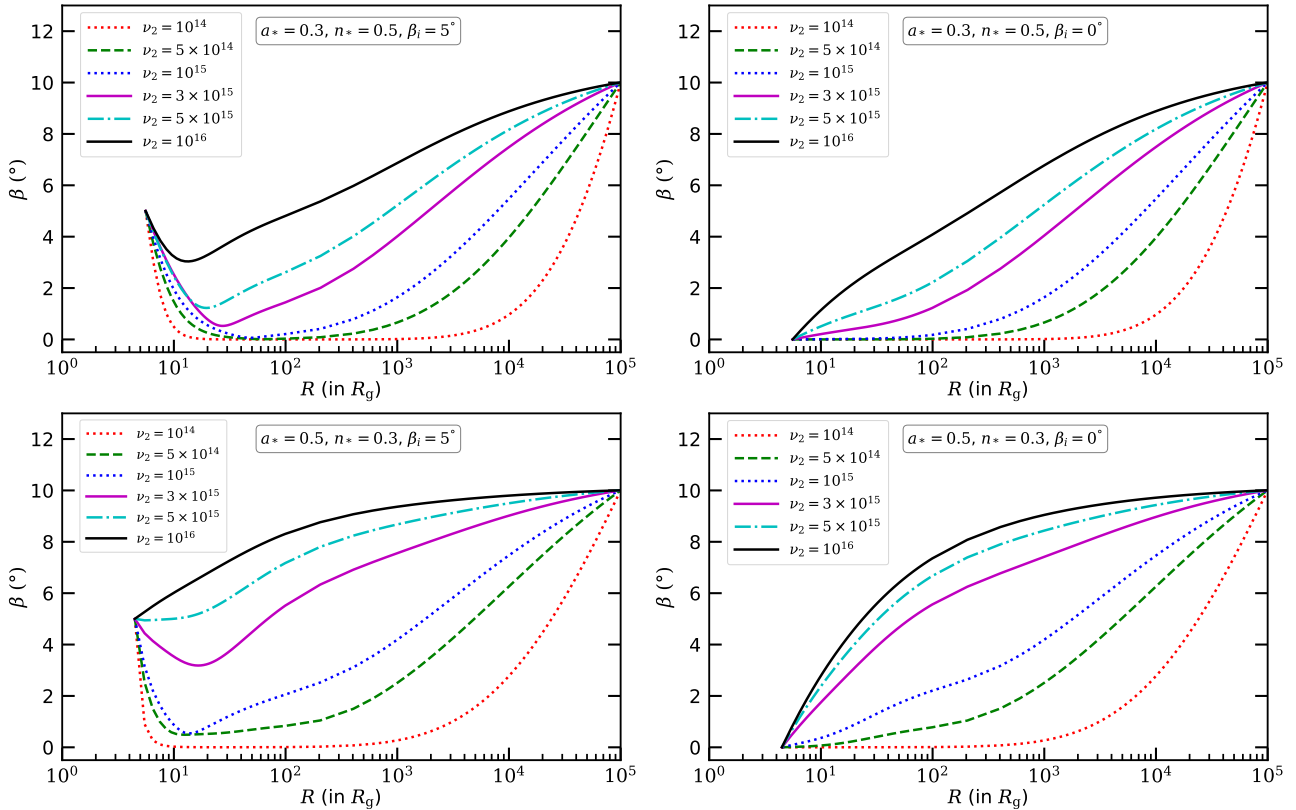


Figure 5: Variation  $\beta$  with  $R$  for different values of  $\nu_2$  with a fixed  $M = 10M_\odot$ ,  $\eta = 0.25$  and  $z_{\text{in}} = 0.75$ . The values of  $a_*$  and  $n_*$  are mentioned in the inset. See § 4 for details.

figure 6 and figure 7, we can infer that when the viscosity parameter  $\nu_2$  (representing viscous torque) is higher, a more massive black hole (higher  $M$ ) is needed to align the disk. This observation highlights the complex relation among the black hole mass, viscous torque, and the alignment dynamics of the accretion disk.

### Warp radius of the disk

It is seen from the above discussion that a disk is partially aligned for a set of parameter values. In such a case, one can consider a radius  $R_{\text{align}}$  up to which the disk remains aligned. It is higher for the higher values of LT effect. In our computation, we consider  $R_{\text{align}}$  as the radius up to which the tilt angle is less than  $0.01^\circ$  following [19]. The characteristic warp radius ( $R_{\text{warp}}$ ) is defined that radius, inside which the LT effect dominates [19]. It is calculated by equating the timescale for warp diffusion (i.e.,  $R^2/\nu_2$ ) and the local LT precession timescale (i.e.,  $1/|\Omega_p|$ ). Thus, one can solve the following equation

$$\left| \left( \frac{2a_*R_g}{R} - \frac{3a_*^2R_g^{3/2}}{2R^{3/2}} - \frac{2n_*^2R_g^{1/2}}{R^{1/2}}(1 - 2R_g/R)^2 \right) \right| = \frac{\nu_2}{cR_g} \quad (32)$$

for  $R = R_{\text{warp}}$  to obtain the warp radius for our case. It gives  $R_{\text{warp}} = 2a_*cR_g^2/\nu_2$  for a slowly-spinning Kerr black hole, which resembles to Eq. (45) of [19]. When the LT effect due to  $n_*$  (3rd term of Eq. 32) dominates over LT effect due to  $a_*$  (1st term of Eq. 32), one has to solve it by considering the negative sign in the right hand side of Eq. (32). Otherwise, it has to be considered as positive. Let us take an

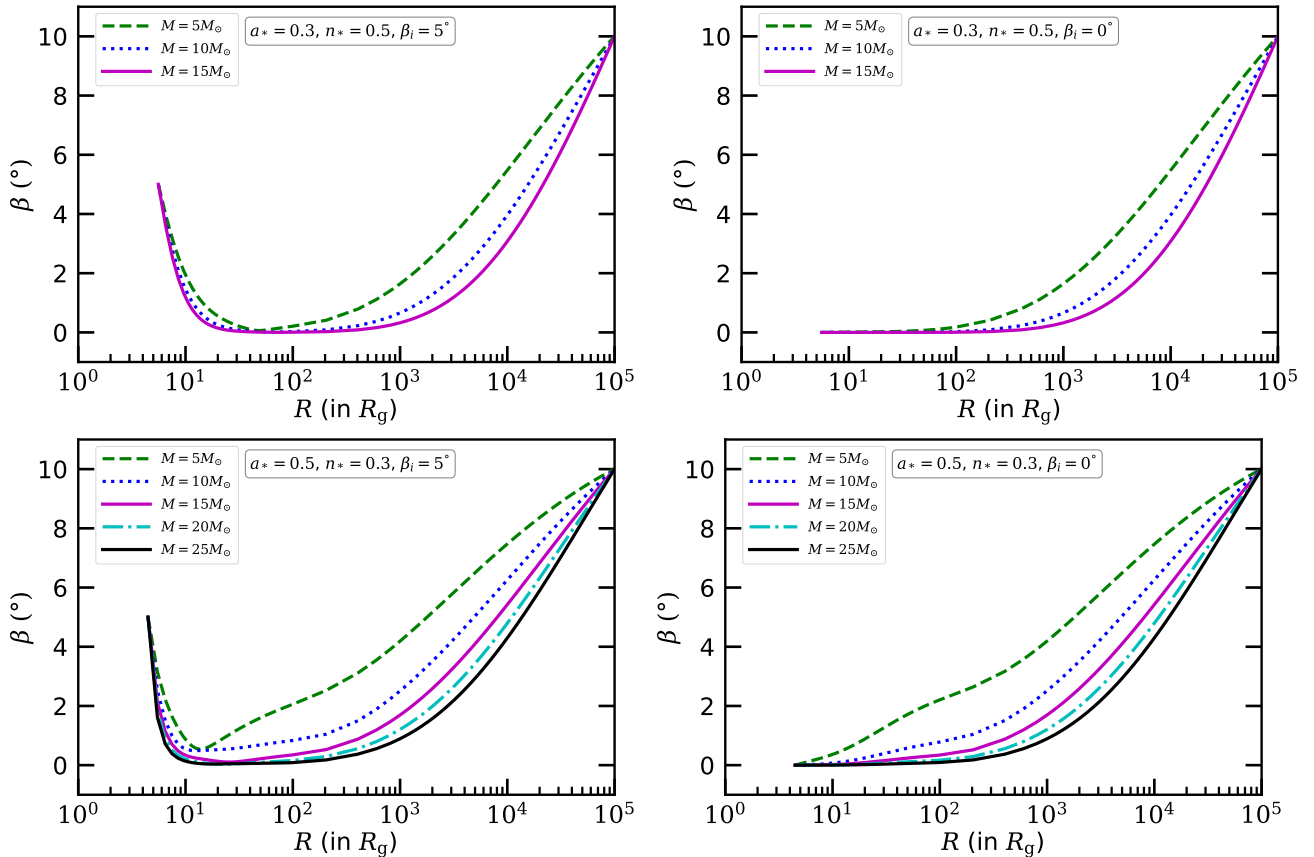


Figure 6: Variation of  $\beta$  with  $R$  for different values of black hole mass ( $M$ ) for a fixed  $\nu_2 = 5 \times 10^{14} \text{ cm}^2 \text{ s}^{-1}$ ,  $\eta = 0.25$  and  $z_{\text{in}} = 0.75$ . The values of  $a_*$  and  $n_*$  are mentioned in the inset. See § 4 for details.

example from the plots of panel (d) of Fig. 2 which corresponds to  $\beta(R)$  for  $M = 10M_\odot$ ,  $a_* = 0.4$  and  $\nu_2 = 10^{15} \text{ cm}^2 \text{ s}^{-1}$  with three different values of  $n_*$ . For  $(a_*, n_*) = (0.4, 0.0)$ , we obtain  $R_{\text{warp}} \sim 34R_g$  by considering the above-mentioned positive sign. Similarly, for  $(a_*, n_*) = (0.4, 0.4)$  and  $(0.4, 0.5)$ , we get  $R_{\text{warp}} \sim 110R_g$  and  $\sim 500R_g$  respectively, by considering the negative sign. Intriguingly, one obtains  $R_{\text{warp}} \sim 13R_g$  for  $(a_*, n_*) = (0.4, 0.3)$  by considering the positive sign. Note that the LT precession vanishes at  $R_0 \sim 24.5R_g$  in this particular case as mentioned earlier. It indicates that the LT effect lost its control over the disk for  $R > 13R_g$ . Moreover, due to  $n_* < a_*$  the third term of Eq. (32) remains small (including the overall LT effect), and cannot take over the control on the disk for  $R > R_0$ . Eventually, the viscous torque dominates the overall LT torque, and  $\beta(R)$  curve starts to move upward.

## 5 Summary and Conclusion

In this paper, we numerically solve the warped accretion disk equations in the viscous regime for a slowly-spinning KTN black hole with a small NUT charge/GMM. Taking into account the inner disk contribution, we obtain the radial profile of the tilted disk around the said black hole starting from the outer edge of the disk upto ISCO radius. We analyze the radial profile of the tilted disk as a function of the several parameters from our numerical results. The alignment of the disk strongly depends on the tug-of-war between the viscous torque (controlled by  $\nu_2$ ) and the LT torque (controlled by  $M$ ,  $a_*$  and  $n_*$ ). In case of the KTN black hole, the LT precession does not monotonically increase with the decrement



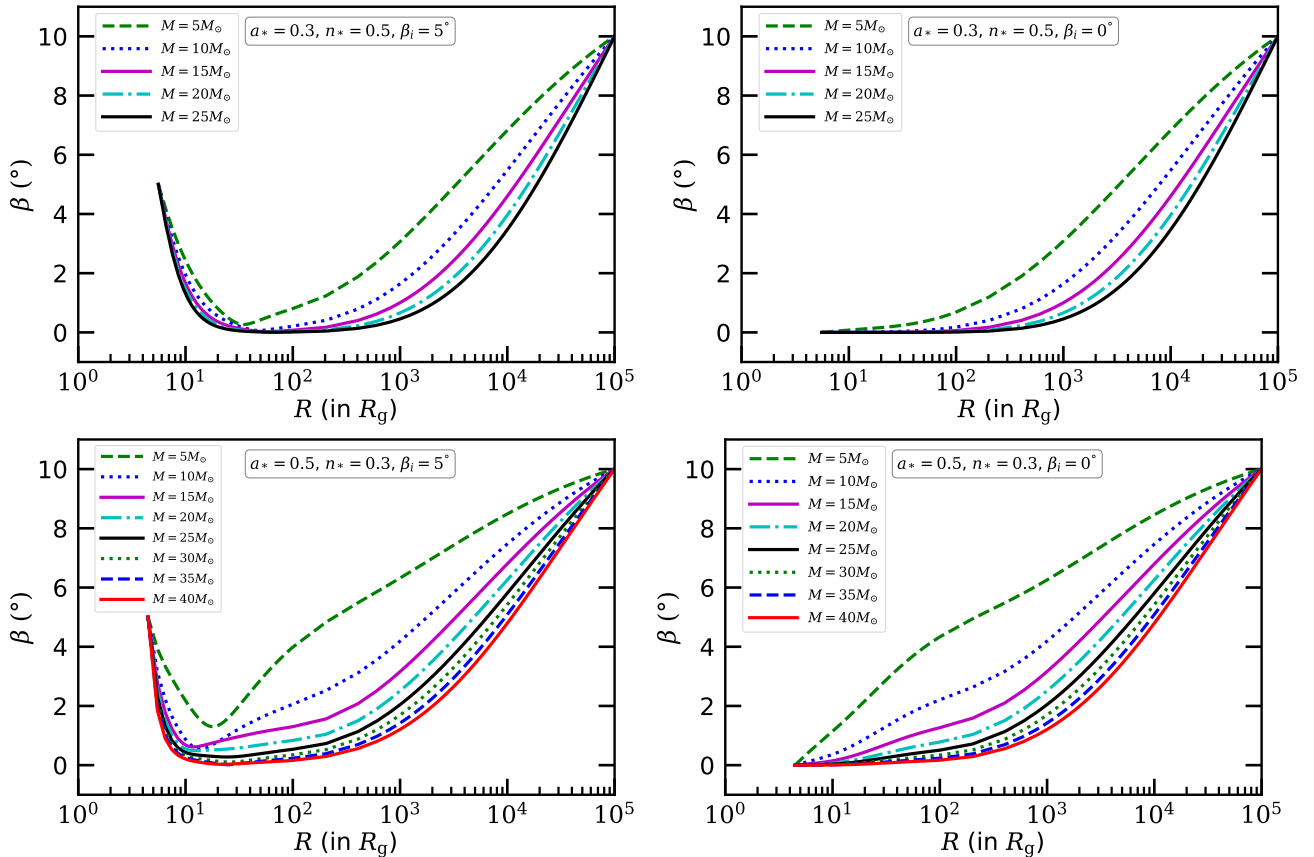


Figure 7: Similar to Fig. 6 but for a fixed  $\nu_2 = 10^{15} \text{ cm}^2 \text{ s}^{-1}$ . See § 4 for details.

of  $R$  towards  $R_{\text{ISCO}}$ , unlike a Kerr black hole. Instead, if the value of  $R$  decreases from the outer orbit to ISCO, the modulus of LT precession frequency first increases, attains a peak, then decreases to zero, and increases again depending on the numerical values of  $(a_*, n_*)$  and the location of ISCO. Therefore, it is evident that the interplay between the LT effects due to  $a_*$  and  $n_*$  is also important in this case. Since, the radial profile of  $\beta$  is also affected by the intriguing behavior of LT effect, the behavior of all curves for  $\beta(R)$  is non-monotonous. We find that the inner disk could be entirely misaligned for a reasonable range of parameter values, which could confront with the astrophysical observations. For specific values of  $M$  and  $\nu_2$ , there are combinations of  $(a_*, n_*)$ , where the disk begins to align with the direction of the black hole spin, indicating that the Bardeen-Petterson effects could be observed.

Certainly, the study of inner accretion disk plays an important role to probe the strong gravity regime. Tilting of the inner accretion disk with respect to the black hole spin axis affects the spectral and timing properties of the X-ray emission through the LT precession, and therefore, it is useful to study the same in strong gravity regime. In fact, C-type low frequency quasi-periodic-oscillation (QPO) frequency is identified as the LT precision frequency [43, 44, 45], and shown to be emerged from the inner accretion disk. Note that a tilted inner disk has been inferred from X-ray spectral and timing features of the accreting black hole H1743-322 [20]. GRO J1655-40 is still misaligned [22]. These misalignment's could be explained employing the present formulation. More importantly, since the existence of GMM is hinted in GRO J1655-40 [6] and M87\* [24], and even in the galaxy [25, 26], our solution for the radial profile of the tilted disk around a KTN black hole could be useful to probe the strong gravity regime as well as the existence of GMM in nature. We plan to study the tilted thin inner accretion disk for the full KTN spacetime in future.



## References

- [1] J. Lense and H. Thirring, *Phys. Z.* **19**, 156 (1918).
- [2] C. Chakraborty, P. Majumdar, *Class. Quantum Grav.* **31**, 075006 (2014).
- [3] R. M. Wald, *General relativity*, The University of Chicago Press, Chicago and London (1984).
- [4] E. Newman, L. Tamburino, T. Unti, *J. Math. Phys.* **4**, 915 (1963).
- [5] C. W. Misner, *J. Math. Phys.* **4**, 924 (1963).
- [6] C. Chakraborty, S. Bhattacharyya, *Phys. Rev. D* **98**, 043021 (2018).
- [7] C. Chakraborty, P. Majumdar, *Eur. Phys. J. C (Letter)* **83**, 714 (2023).
- [8] C. Chakraborty, B. Mukhopadhyay, *Eur. Phys. J. C* **83**, 937 (2023).
- [9] W. B. Bonnor, *Proc. Camb. Phil. Soc.* **66**, 145 (1969).
- [10] J. S. Dowker, *Gen. Rel. Grav.* **5**, 603 (1974).
- [11] J. M. Bardeen, J. A. Petterson, *ApJ* **195**, L65 (1975).
- [12] S. P. Hatchett, M. C. Begelman, C. L. Sarazin, *ApJ* **247**, 677 (1981).
- [13] J. A. Petterson, *ApJ* **214**, 550 (1977).
- [14] J. A. Petterson, *ApJ* **218**, 783 (1977).
- [15] J. A. Petterson, *ApJ* **216**, 827 (1977).
- [16] J. E. Pringle, *MNRAS* **258**, 811 (1992).
- [17] P. A. G. Scheuer, R. Feiler, *MNRAS* **282**, 291 (1996).
- [18] C. Chakraborty, S. Bhattacharyya, *MNRAS* **469**, 3062 (2017).
- [19] S. Banerjee, C. Chakraborty, S. Bhattacharyya, *ApJ* **870**, 95 (2019).
- [20] A. Ingram et al., *MNRAS* **461**, 1967 (2016).
- [21] C. Chakraborty, S. Bhattacharyya, *JCAP* 05(2019)034.
- [22] R. G. Martin, R. C. Reis, J. E. Pringle, *MNRAS*, 391, L15 (2008).
- [23] C. Chakraborty, S. Bhattacharyya, *Phys. Rev. D* **106**, 103028 (2022).
- [24] M. Ghasemi-Nodehi, C. Chakraborty, Q. Yu, Y. Lu, *Eur. Phys. J. C* **81**, 939 (2021).
- [25] J. Govaerts, *Class. Quantum Grav.* **40**, 085010 (2023).
- [26] M. L. Ruggiero, *JCAP* 02(2024)025.
- [27] D. Lynden-Bell, M. Nouri-Zonoz, *Rev. Mod. Phys.* **70**, 427 (1998).
- [28] I. K. Dihinia et al., *Phys. Rev. D* **102**, 023012 (2020).

- [29] S. Ramaswamy, A. Sen, Phys. Rev. Lett. **57**, 1088 (1986).
- [30] G. Clément, D. Gal'tsov, M. Guenouche, Phys. Lett. **B 750**, 591 (2015).
- [31] G. Clément, D. Gal'tsov, M. Guenouche, Phys. Rev. **D 93**, 024048 (2016).
- [32] R. A. Hennigar, D. Kubiznák, R. B. Mann, Phys. Rev. **D 100**, 064055 (2019).
- [33] A. B. Bordo, F. Gray, D. Kubiznák, J. High Energy Phys. **2019**, 119 (2019).
- [34] J. G. Miller, J. Math. Phys. (N.Y.) **14**, 486 (1973).
- [35] S. Kato, PASJ **42**, 99 (1990).
- [36] C. Chakraborty, P. Kocherlakota, M. Patil, S. Bhattacharyya, P. S. Joshi, A. Królak, Phys. Rev. **D 95**, 084024 (2017).
- [37] N. I. Shakura, R. A. Sunyaev, A&A, **24**, 337 (1973).
- [38] J. C. B. Papaloizou, J. E. Pringle. MNRAS **202**, 1181 (1983).
- [39] G. I. Ogilvie, Mon. Not. Roy. Astron. Soc. **304**, 557 (1999).
- [40] T. Fragos, T., J. E. McClintock, ApJ **800**, 17 (2015).
- [41] J. Frank, A. R. King, D. Raine, Accretion Power in Astrophysics, 3rd Edition, Cambridge University Press (2002).
- [42] A. R. King, J. E. Pringle, M. Livio, MNRAS **2007**, 376, 1740.
- [43] L. Stella, M. Vietri, ApJ **492**, L59 (1998).
- [44] L. Stella, M. Vietri, Phys. Rev. Lett. **82**, 17 (1999).
- [45] A. Ingram, S. Motta, MNRAS **444**, 2065 (2014).